

Online Research @ Cardiff

This is an Open Access document downloaded from ORCA, Cardiff University's institutional repository: <https://orca.cardiff.ac.uk/id/eprint/100397/>

This is the author's version of a work that was submitted to / accepted for publication.

Citation for final published version:

Turner, Matthew, Deeth, Robert J. and Platts, James Alexis ORCID: <https://orcid.org/0000-0002-1008-6595> 2017. Prediction of ligand effects in platinum-amyloid- β coordination. *Journal of Inorganic Biochemistry* 173 , pp. 44-51. 10.1016/j.jinorgbio.2017.05.003 file

Publishers page: <http://dx.doi.org/10.1016/j.jinorgbio.2017.05.003>
<<http://dx.doi.org/10.1016/j.jinorgbio.2017.05.003>>

Please note:

Changes made as a result of publishing processes such as copy-editing, formatting and page numbers may not be reflected in this version. For the definitive version of this publication, please refer to the published source. You are advised to consult the publisher's version if you wish to cite this paper.

This version is being made available in accordance with publisher policies.

See

<http://orca.cf.ac.uk/policies.html> for usage policies. Copyright and moral rights for publications made available in ORCA are retained by the copyright holders.



Prediction of Ligand Effects in Platinum-Amyloid- β Coordination

Matthew Turner^a, Robert J. Deeth^b and James A. Platts^{a*}

^a School of Chemistry, Cardiff University, Park Place, Cardiff CF10 3AT

^b Department of Chemistry, University of Warwick, Gibbet Hill, Coventry, CV4 7AL

* Corresponding Author: Dr. James A. Platts, School of Chemistry, Cardiff University, Park Place, Cardiff CF10 3AT, UK. Email: platts@cardiff.ac.uk; Phone: +44-2920-874950

Abstract

Ligand field molecular mechanics (LFMM) and semi-empirical Parametric Model 7 (PM7) methods are applied to a series of six Pt^{II}-Ligand systems binding to the N-terminal domain of the amyloid- β (A β) peptide. Molecular dynamics using a combined LFMM/Assisted Model Building with Energy Refinement (AMBER) approach is used to explore the conformational freedom of the peptide fragment, and identifies favourable platinum binding modes and peptide conformations for each ligand investigated. Platinum coordination is found to depend on the nature of the ligand, providing evidence that binding mode may be controlled by suitable ligand design. Boltzmann populations at 310K indicate that each Pt-A β complex has a small number of thermodynamically accessible states. Ramachandran maps are constructed for the sampled Pt-A β conformations and secondary structural analysis of the obtained complex structures is performed and contrasted with the free peptide; coordination of these platinum complexes disrupts existing secondary structure in the A β peptide and promotes formation of ligand-specific turn-type secondary structure.

Introduction

Alzheimer's disease (AD) is a neurodegenerative condition associated with progressive cognitive decline in patients and is the most common cause of late-life dementia¹. The causes and development of AD are poorly understood, as the disease involves a variety of physiological processes². The two main hallmarks of AD are the presence of extracellular plaques and intracellular neurofibrillary tangles³. Amyloid- β ($A\beta$) peptide was first identified as a key component of these plaques in 1985⁴, and has become the focus of much research interest in possible AD-therapeutics. The amyloid-cascade hypothesis^{3,5,6,7,8,9} suggests that $A\beta$ monomers aggregate to form these plaques, which are widely believed to be one of the key drivers of the condition. As a result, the early stages of the $A\beta$ aggregation process have become a target for the development of AD-therapeutics².

$A\beta$ monomers are usually 40 or 42 residues long and contain a hydrophilic N-terminal domain with high-affinity metal binding sites, particularly the His-rich region at residues 1-16. This region of $A\beta$ has been widely reported as being responsible for physiological coordination of transition metals such as copper. However, there appears to be some breakdown in the metal transport mechanisms in the AD process, as analysis of amyloid deposits has shown increased concentrations of these transition metal ions,^{10,11} suggesting that these metals are important in the development of $A\beta$ plaques. To date, metal binding sites have not been clearly defined, with many authors demonstrating different metal coordination, although the N-terminal histidine residues (His6, His13, His14) appear frequently.^{12,13,14,15} One possible route to AD-therapeutics involves disrupting the coordination of the physiological metal ions using compounds that selectively occupy the transition metal binding sites, thereby hindering the $A\beta$ aggregation process. To this end, Barnham *et al.*^{16,17} showed that Pt^{II} (phenanthroline)

complexes are able to inhibit A β aggregation and limit its neurotoxicity *in vitro*. The presence of aromatic ligands appears to be important for activity, as these ligands show some affinity for A β ¹⁸ and are able to form stabilising π - π interactions with residues Phe, Tyr and His¹⁸ while the archetypal Pt^{II} drug cisplatin is inactive towards A β aggregation. In addition, these Pt^{II} complexes are not toxic at the concentrations required to inhibit the aggregation of A β ¹⁶.

However, characterization of these Pt^{II}(ligand)-A β complexes is difficult, with authors suggesting a variety of different metal binding modes^{16,19,20}. Experimental evidence indicates that a series of platinated adducts are formed when Pt^{II}(phenanthroline) complexes bind to A β , though the N-terminal His6 and His14 residues are the most common Pt^{II} binding sites^{16,19,20,21}. Computational approaches may provide clear insight into this problem, without the need for complex synthesis. Of particular note is work by Streltsov *et al.*, which combined Extended X-ray Absorption Fine Structure (EXAFS) and Density Functional Theory (DFT) data for a series of model Pt^{II} complexes to provide predictions of metal-a β binding modes²².

However, computational modelling of these metal-peptide systems is challenging; quantum mechanical (QM) methods are not typically applied to the study of large, flexible peptide systems such as A β for reasons of computational cost, while classical modelling techniques (*i.e.* molecular mechanics (MM)) do not model the influence of metal d-shell electrons on the structure and properties of transition metal coordination complexes²³. Alternatively, ligand field molecular mechanics (LFMM)^{24,25,26} appears well-suited to the study of these transition metal – biomolecule interactions, by introducing a Ligand Field Stabilisation Energy (LFSE) term into the construction of the forcefield in order to handle the d-orbital electron effects. This gives LFMM ‘*the flexibility and generality of quantum mechanics with the speed of molecular mechanics.*’²³ which has allowed success in the modelling of a range of Jahn-Teller active Cu^{II} systems²⁷, spin states of Ni and Fe complexes²⁸ as well as some Pt^{II}-biomolecule studies^{29,30,31}.

The aim of this work is to generate and subsequently analyse conformations of a series of Pt^{II} species bound to a fragment of A β peptide (residues 6-14 – see Figure 1), in order to identify favourable platinum-binding modes and peptide conformations. This peptide was chosen for study as it contains the N-terminal residues necessary to study transition metal binding, and is sufficiently small to allow calibration of findings through use of DFT. This work presents findings for six platinum-ligand systems (see Figure 2), which stem from recent literature. The modelling approaches outlined here may be extended to study other ligands²⁰, other transition-metal based therapeutics of current research interest (*e.g.* ruthenium³² and mixed-metal complexes^{33,34}).

Computational Methods

The peptide sequence His6-Asp-Ser-Gly-Tyr-Glu-Val-His-His14 was built in an extended conformation in Molecular Operating Environment (MOE)³⁵, and protonation states at pH of 7.4 assigned using the Protonate3D module of this package. Pt^{II}(ligand) complexes were manually constructed and bound to the peptide in eight distinct binding modes from all combinations of N δ / N ϵ of His6 and His13/His14. For conformational searching, complexes were described using a combination of ligand field molecular mechanics (LFMM) for Pt^{II}^{23,29,30} and Assisted Model Building with Energy Refinement (AMBER94)³⁶ parameters for all other atoms, as implemented in the d-orbital extension to MOE (DommiMOE)²⁶. Partial charges were calculated for model Pt^{II}(imidazole)₂(ligand) systems using the Merz-Kollman scheme from HF/6-31G(d)/SDD electrostatic potential in Gaussian09³⁷, with Pt^{II} given a van der Waals radius of 2.0 Å. The remaining peptide atoms were assigned AMBER94 charges as calculated by MOE. Solvation effects were modelled using the reaction-field model with default parameters.

Conformational freedom was explored via the LowMode MD (LMMD)³⁸ method in MOE. LMMD searches were configured to terminate after 100 successive failures to generate a new conformation up to a maximum of 10,000 iterations, with a large energy cut-off (10,000 kcal/mol) and a Root-Mean-Square Deviation (RMSD) cut-off of 0.25 Å used for removal of any duplicate conformations. During the LMMD search, the platinum centre was set at a fixed potential to avoid premature termination of the conformational search.³¹ Semi-empirical calculations were performed using the Molecular Orbital PACKage (MOPAC) in its 2012³⁹ version, with the Parametric Model 7 (PM7) method⁴⁰ and the Conductor-like Screening Model (COSMO) model of aqueous solvation⁴¹. Overlay plots and images were obtained using Chimera imaging software⁴². Ramachandran maps were plotted using the JMP statistical package⁴³.

Results and Discussion

In this work, we generate and analyse conformations of a series of Pt^{II} species (see Figure 2) bound to a fragment of A β peptide, with the aim of identifying favourable metal-binding modes and peptide conformations. Using the protocol outlined above, we performed conformational searches on each platinum binding mode for all ligand systems (8 for the symmetric ligands 1 - 4; 16 for asymmetric ligands 5 and 6). This produced a large number of possible conformers for each platinum binding mode (Table 1).

There is significant variation in the number of conformations found between these different ligands and coordination modes, which may be partly due to the stochastic nature of the LMMD search as well as the effect of different complexes/coordination modes on peptide flexibility. In comparison, an identical simulation using the free peptide fragment produced 9962 conformations, emphasising the fact that coordination of these platinum complexes greatly reduces the conformational freedom of A β ³¹.

It is particularly notable that both asymmetric ligands produced significantly greater numbers of possible structures than their symmetric counterparts. While some of this difference may be attributed to the increased number of conformational searches required for these systems, *i.e.* two different simulations for the two orientations of the ligands, with the ligand 5-membered ring *cis*- or *trans*- to His6, this does not explain the large numbers of structures identified for certain coordination modes. This greater number of conformations suggests that these ligands do not restrict the flexibility of A β to the same extent as the first four ligands. It is also notable that the number of conformations for a given coordination mode are similar (ratios 0.76-1.27, Table 1), but vary dramatically across the ligand series (ratios 0.57-2.67). This suggests that the nature of the ligand affects the flexibility of A β more than the coordination mode.

As we have shown previously,³¹ PM7/COSMO optimization of each conformation is able to provide both accurate geometries and relative energies of these systems. We therefore performed this step for all conformations identified above, a total of over 52,000 conformations. The resulting relative energies were collated and used in Boltzmann weighting calculations to determine the binding mode(s) and conformation(s) that contribute significantly to the overall ensemble at 310 K, the results of which are reported in Table 2. While low energy conformations are the main focus of this work, we note that the range of relative energy of conformations found in this process is large: the maximum PM7 energy is (1): 583, (2): 403, (3): 233, (4): 372, (5): 657, (6): 726 kJmol⁻¹. That such high-energy conformations survive LFMM followed by PM7 optimization is slightly surprising, but gives us reassurance that the conformational freedom of the peptide has been sampled. We also note that PM7 optimization resulted in between 10 and 20 (1 to 2%) of conformations reported in Table 1 no longer being unique, a small value that attests to the quality of the geometries that result from LFMM.

On the basis of these results, we predict that the binding of Pt^{II} to histidine residues is strongly dependent on the identity of the ligand, though these systems exhibit some preference for Pt^{II}-binding via N ϵ rather than N δ in His residues. This appears to be an inherent property of the histidyl residue: calculations on a series of model Pt^{II}(Ligand)(Cl)His complexes using PM7 gives preference for N ϵ binding in His residues, except in the case of ligands **4** and **6**, where His binding via N δ is strongly favoured (see Table 3). However, the relative stability of N ϵ vs. N δ binding in these model systems is not always reflected in the full peptide systems (see Table 2, with particular emphasis on ligand **6**) *i.e.* this preference can be overcome by stabilising other binding modes with π - π interactions and/or low strain peptide conformations.

In the model systems using asymmetric ligands (**5** and **6**) the orientation of the ligands appears to be important; the coordination of ligand **5** when His coordinates *trans*- to the 6-membered ring is significantly more stable than when His coordinates *cis*- to the 6-membered ring (see Figure 2 for reference). Interestingly, while N ϵ binding is favoured by approximately the same amount in the first two ligand systems, there is very little energy difference between the N δ /N ϵ binding for the ligand **3**. This may go some way to explaining the mixed N δ /N ϵ coordination mode seen in the low energy conformations (Table 2).

Furthermore, the orientation of the ligand remains important in the full peptide systems: in the case of ligand **5**, the lowest energy conformation where His6 coordinates *trans*- to the 6-membered ring rather than the 5-membered ring is located 46 kJ/mol above the most stable conformer. Similarly, in the case of ligand **6**, the first conformation identified where His6 coordinates *trans*- to the 6-membered ring appears 49 kJ/mol above the minimum energy conformer.

The data in Table 2 also indicate that a very small number of conformations contribute significantly to the Boltzmann-weighted ensemble at 310K. For ligands 1, 3 and 4, a single conformer dominates the ensembles, whereas for 2, 5 and 6 several conformers are predicted to co-exist with significant probability. The alternative low energy conformations of these complexes are discussed in more detail below. These results are consistent with our previous findings and reinforce the assertion that coordination of these Pt^{II} complexes greatly reduces conformational freedom of Aβ³¹. The low energy conformations identified in Table 2 are shown in Figure 3. Table 2 also shows there is distinct preference in coordination mode for each of the ligands studied; this coordination is summarised in Table 4 below. This is a promising result in the case of ligand 2 since the metal binding mode we identify as the most favourable (His6 ε – His14 ε) agrees with existing experimental data obtained by Ma *et al.*¹⁹ This also suggests that changing the ligand bound to platinum is able to influence the preferred Pt^{II}-binding mode and thus, that the binding mode may be controlled through choice and design of the ligand.

To investigate these results further, we focus on two structural features: i) Pt^{II} coordination and ii) peptide backbone geometry in order to assess the range of geometries sampled in the conformational searching process, and to identify any features of low energy conformations.

The calculated bond lengths and angles around the central platinum in each ligand system are summarised in Table 5. These data show that there is little variation in Pt—N_{His} bond lengths following change in conformation and/or coordinated ligand, but that there is notable variation of the Pt-N_{Lig} bond distances across the range of ligands. Additionally, these data show that there is a systematic difference in length of the Pt-N_{Lig} and Pt-N_{His} bonds – specifically the

average Pt-N_{His} bond distances are slightly shorter than the corresponding Pt-N_{Lig} bond distances. However, comparison with the geometrical data for the low energy conformations (Table 5) clearly shows that these stable structures are not significantly different from the average conformation in each case, suggesting that the platinum geometry is not especially important in determining complex stability. It is also notable that these Pt—N distances are in good agreement with those of Streltsov *et al.*²² for ligand **2**, who reported Pt–N(imidazole) and Pt–N(phen) bond distances of 2.03(1) Å and 1.993(5) Å, respectively, as well as confirming the square planar coordination of this ligand to amino acids.

Backbone dihedral angles for all conformations were calculated, allowing Ramachandran plots to be constructed. This allows us to identify any secondary structure forming within the usually random coil N-terminal region of A β . The free A β 6-14 fragment was modeled using an identical protocol, which identified 9962 possible conformations; backbone dihedrals for these conformations were calculated and used to produce a Ramachandran map using JMP⁴³ (See Figure 4). In agreement with previous findings,^{46,47,48,49} this fragment of the A β peptide is highly flexible, illustrated by the wide coverage of the Ramachandran plot. Conformations are concentrated around two distinct right-handed helical regions of conformational space, with smaller contributions from β -sheet and turn regions. Values of ϕ/ψ for the lowest energy conformation located are reported in Table 6, and secondary structure assigned by STRIDE⁵⁰ in Table 7. Despite occupying the region of ϕ/ψ space expected for helices, residues are best described as turn/coil due to lack of H-bonding expected in α - and 3_{10} -helices, in agreement with the findings of Yang and Teplow⁴⁹. Those authors also identified ‘*highly populated turn structures, centred at [residues] 6-9*’ of the free A β peptide, and highlighted the importance of such turns for aggregation.

Ramachandran plot were then generated for each Pt^{II}(ligand) system studied. For example, Figure 5 shows that for the favoured His6 ϵ - His14 ϵ coordination of the platinum complex with ligand **2**, conformations cover a similar range to that observed for the free peptide, but the concentration of residues in the right-handed helical region is reduced, with much greater scatter of ϕ/ψ in the area expected for helical peptides, including a significant contribution at negative ϕ /positive ψ . Moreover, the Pt(**2**) complex exhibits a greater propensity for turn-like structures centred around +70/-60°. Analogous plots for each coordination mode with ligand **2** (see SI) illustrate Ramachandran maps are broadly similar regardless of platinum binding mode. As noted above, three complexes exhibit multiple low-energy conformations: backbone dihedrals for alternative conformations are reported in ESI (Table S1). In all cases, the second lowest energy conformation has similar backbone conformation to the lowest energy one, and in Pt(**6**) especially the third conformation differs only in one angle of one residue (Tyr10). Thus, even in cases where multiple conformations are identified the overall flexibility of the peptide backbone is still very restricted.

However, as illustrated in Table 2, many of the generated conformations are of relatively high energy, so are of little biological relevance. The peptide geometries within these low energy conformations are summarized in Table 6. Analysis of these conformations using STRIDE to identify any secondary structure elements was performed and results shown in Table 7. Data for the free peptide are in agreement with previous findings⁴⁹ of a turn in residues 5 – 9, with coil-like structure in residues 10-14. In general, a clear picture of disruption of the free peptide's turn between residues 5 and 10 emerges from this analysis. The detailed effect of platination on this pattern varies with ligand: in most cases, a mix of turn and coil values are found, but the location of the turn residues changes. Pt(**3**) is probably the closest to the free peptide but truncates the observed turn by two residues, whereas Pt(**2**), Pt(**4**) and Pt(**6**) move

the turn later in the sequence. Interestingly, STRIDE identifies a short stretch of 3_{10} -helix in the low energy Pt(1) structure, while Pt(5) is assigned as almost completely turn in nature.

Conformations were also analysed for close contacts between peptide and ligand, defined as the distance between C_γ in a residue and a C atom in the centre of the ligand. This revealed that Tyr10 in particular forms numerous contacts with ligands, and that such contacts are more prevalent in the favoured coordination modes than in alternative forms. Full details of intramolecular distances can be found in supporting information: as an example, Figure 6 compares such contacts between the favoured coordination mode and the next most stable for Pt(1) and Pt(2). In both cases, the favoured coordination mode exhibits a distribution skewed towards short distances between ligand and Tyr10. The situation is less clear cut for other ligands, but in general the favoured coordination mode has on average one of the shortest contact distances. We speculate, therefore, that such formation of such contacts are one of the main factors in determining how a particular ligand system alters how platinum binds to A β .

Conclusions

LFMM is a powerful modelling tool for the study of transition metal complexes and has previously found success in predicting their interactions with biomolecules. In this work, we apply the LFMM approach to a series of six Pt^{II} complexes - as studied by Barnham^{16,17,45} and others^{19,20,21} - and their interaction with model fragments of the amyloid- β peptide in order to determine favourable metal binding modes as well as their influence on peptide secondary structure. Conformational space of A β was explored using LowMode MD with AMBER

molecular mechanics parameters, followed by further optimisation using the semi-empirical PM7 method.

Boltzmann populations for each conformation were calculated at 310K and favourable platinum binding modes were identified for each complex studied. The preferred binding mode was found to be dependent on the nature of the ligand, with varied N δ or N ϵ coordination across the N-terminal histidine residues of A β . These changes in binding mode suggest that the platinum coordination may be controlled via the choice of the ligand. Furthermore, the Boltzmann populations for these complexes indicate that a small number of conformations contribute significantly to the ensemble at 310K, suggesting that the flexibility of the peptide is severely reduced after coordination of these platinum complexes.

Analysis of the platinum coordination geometry illustrated that the low energy conformations were not significantly different from the average across databases, meaning that their stability is likely conferred by the peptide conformation rather than the metal geometry, and in particular close contacts between residue side chains the planar ligands. It is surprising that such ligands, which differ only slightly in their steric and electronic nature, effect such large changes on coordination and conformation. The available peptide conformations were plotted as Ramachandran maps, allowing for identification of secondary structure elements within the peptide. While the N-terminal region of A β is known to be disordered, the most stable conformation of the free peptide found here was shown to exhibit turn-type secondary structure in residues His6-Glu11. Coordination of each platinum-ligand complex disrupts this secondary structure differently, including interrupting or translating the existing turn-type structure as well as formation of a short 3,10-helix. Restricting the conformational freedom and disrupting the secondary structure of A β may have consequences for the effect of these complexes on limiting aggregation, for instance by hindering the formation of β -sheet structures known to be important in plaques.

In future, there are several research avenues to be pursued. Firstly, the peptide system will be extended to more biologically relevant 1-16, 1-28 subunit and the full peptide. In addition, the modelling approaches outlined here may be applied to the study of cyclo-metalated ligands such as those of Collin et al²⁰. Alternatively, the LFMM procedure may be applied to other transition-metal based therapeutics (*e.g.* ruthenium³² and mixed-metal complexes³³) or the physiologically important copper, iron and zinc ions³⁴, though these approaches may require the development of new LFMM parameters.

Acknowledgements

This work was carried out using resources of the Advanced Research Computing @ Cardiff (ARCCA) and HPC Wales facilities. MT is grateful to Cardiff University for a studentship. RJD acknowledges the University of Edinburgh for granting an Honorary Fellowship. Molecular graphics were obtained using the UCSF Chimera package, except Figure 1 which was generated with Inkscape. Chimera is developed by the Resource for Biocomputing, Visualization, and Informatics at the University of California, San Francisco (supported by NIGMS P41-GM103311). RJD acknowledges the support of Chemical Computing Group.

Supporting Information.

Ramachandran plots for different coordination modes, backbone dihedrals of low energy conformations, non-bonded contact distances and Cartesian coordinates of predicted low energy structures can be found in ESI.

References

- 1 B. L. Plassman, K. M. Langa, G. G. Fisher, S. G. Heeringa, D. R. Weir, M. B. Ofstedal, J. R. Burke, M. D. Hurd, G. G. Potter, W. L. Rodgers, D. C. Steffens, R. J. Willis and R. B. Wallace, *Neuroepidemiology*, 2007, 29, 125–132.
- 2 D. Valensin, C. Gabbiani and L. Messori, *Coord. Chem. Rev.*, 2012, 256, 2357–2366.
- 3 D. Selkoe, *Neuron*, 1991, 6, 487–498.
- 4 C. Masters, G. Simms, N. Weinman, G. Multhaup, B. McDonald and K. Beyreuther, *Proc. Natl. Acad. Sci. U. S. A.*, 1985, 82, 4245–4249.

- 5 D. M. Walsh, I. Klyubin, J. V. Fadeeva, W. K. Cullen, R. Anwyl, M. S. Wolfe, M. J. Rowan and D. J. Selkoe, *Nature*, 2002, 416, 535–539.
- 6 C. Haass and B. De Strooper, *Science*, 1999, 286, 916–919.
- 7 J. P. Cleary, D. M. Walsh, J. J. Hofmeister, G. M. Shankar, M. A. Kuskowski, D. J. Selkoe and K. H. Ashe, *Nat. Neurosci.*, 2005, 8, 79–84.
- 8 J. Hardy and G. Higgins, *Science*, 1992, 256, 184–185.
- 9 J. Hardy and D. J. Selkoe, *Science*, 2002, 297, 353–356.
- 10A. I. Bush, *Trends Neurosci.*, 2003, 26, 207–214.
- 11K. J. Barnham, C. L. Masters and A. I. Bush, *Nat. Rev. Drug Discov.*, 2004, 3, 205–214.
- 12S. Bolognin, L. Messori, D. Drago, C. Gabbiani, L. Cendron and P. Zatta, *Int. J. Biochem. Cell Biol.*, 2011, 43, 877–885.
- 13V. B. Kenche and K. J. Barnham, *Br. J. Pharmacol.*, 2011, 163, 211–219.
- 14S. Zirah, S. A. Kozin, A. K. Mazur, A. Blond, M. Cheminant, I. Segalas-Milazzo, P. Debey and S. Rebuffat, *J. Biol. Chem.*, 2006, 281, 2151–2161.
- 15P. Giannozzi, K. Jansen, G. La Penna, V. Minicozzi, S. Morante, G. Rossi and F. Stellato, *Metallomics*, 2012, 4, 156–165.
- 16K. J. Barnham, V. B. Kenche, G. D. Ciccotosto, D. P. Smith, D. J. Tew, X. Liu, K. Perez, G. A. Cranston, T. J. Johanssen, I. Volitakis, A. I. Bush, C. L. Masters, A. R. White, J. P. Smith, R. A. Cherny and R. Cappai, *Proc. Natl. Acad. Sci. U. S. A.*, 2008, 105, 6813–6818.
- 17K. J. Barnham, V. B. Kenche, L. W. Hung, K. Perez, I. Volitakes, G. Ciccotosto, J. Kwok, N. Critch, N. Sherratt, M. Cortes, V. Lal, C. L. Masters, K. Murakami, R. Cappai and P. A. Adlard, *Angew. Chem.-Int. Ed.*, 2013, 52, 3374–3378.

- 18 S. G. Yao, R. A. Cherny, A. I. Bush, C. L. Masters and K. J. Barnham, *J. Pept. Sci.*, 2004, 10, 210–217.
- 19 G. Ma, F. Huang, X. Pu, L. Jia, T. Jiang, L. Li and Y. Liu, *Chem.-Eur. J.*, 2011, 17, 11657–11666.
- 20 F. Collin, I. Sasaki, H. Eury, P. Faller and C. Hureau, *Chem. Commun.*, 2013, 49, 2130–2132.
- 21 G. Ma, E. Wang, H. Wei, K. Wei, P. Zhu and Y. Liu, *Metallomics*, 2013, 5, 879.
- 22 V. A. Streltsov, V. Chandana Epa, S. A. James, Q. I. Churches, J. M. Caine, V. B. Kenche and K. J. Barnham, *Chem. Commun.*, 2013, 49, 11364.
- 23 R. J. Deeth, A. Anastasi, C. Diedrich and K. Randell, *Coord. Chem. Rev.*, 2009, 253, 795–816.
- 24 V. Burton, R. Deeth, C. Kemp and P. Gilbert, *J. Am. Chem. Soc.*, 1995, 117, 8407–8415.
- 25 V. J. Burton and R. J. Deeth, *J. Chem. Soc. Chem. Commun.*, 1995, 573–574.
- 26 R. J. Deeth, N. Fey and B. Williams–Hubbard, *J. Comput. Chem.*, 2005, 26, 123–130.
- 27 R. J. Deeth and L. J. A. Hearnshaw, *Dalton Trans.*, 2006, 1092–1100.
- 28 R. J. Deeth and K. Randell, *Inorg. Chem.*, 2008, 47, 7377–7388.
- 29 A. E. Anastasi and R. J. Deeth, *J. Chem. Theory Comput.*, 2009, 5, 2339–2352.
- 30 H.-C. Tai, R. Brodbeck, J. Kasparikova, N. J. Farrer, V. Brabec, P. J. Sadler and R. J. Deeth, *Inorg. Chem.*, 2012, 51, 6830–6841.
- 31 M. Turner, J. A. Platts and R. J. Deeth, *J. Chem. Theory Comput.*, 2016, 12, 1385–1392.
- 32 D. Valensin, P. Anzini, E. Gaggelli, N. Gaggelli, G. Tamasi, R. Cini, C. Gabbiani, E. Michelucci, L. Messori, H. Kozlowski and G. Valensin, *Inorg. Chem.*, 2010, 49, 4720–4722.

- 33 V. Rangachari, A. Kumar, L. Moody, J. F. Olaivar, N. A. Lewis, R. L. Khade, A. A. Holder and Y. Zhang, *Acs Chem. Neurosci.*, 2010, 1, 691–701.
- 34 C. J. Maynard, A. I. Bush, C. L. Masters, R. Cappai and Q. X. Li, *Int. J. Exp. Pathol.*, 2005, 86, 147–159.
- 35 Molecular Operating Environment (MOE), (2013.08), Chemical Computing Group Inc., 1010 Sherbooke St. West, Suite #910, Montreal, QC, Canada, H3A 2R7, 2013.
- 36 W. Cornell, P. Cieplak, C. Bayly, I. Gould, K. Merz, D. Ferguson, D. Spellmeyer, T. Fox, J. Caldwell and P. Kollman, *J. Am. Chem. Soc.*, 1995, 117, 5179–5197.
- 37 M. J. Frisch and G. W. Trucks et al., *Gaussian09*, Gaussian Inc., Wallingford, CT, 2009.
- 38 P. Labute, *J. Chem. Inf. Model.*, 2010, 50, 792–800.
- 39 J. J. P. Stewart, <http://openmopac.net/index.html>.
- 40 J. J. P. Stewart, *J. Mol. Model.*, 2013, 19, 1–32.
- 41 A. Klamt and G. Schüürmann, *J. Chem. Soc. Perkin Trans. 2*, 1993, 799–805.
- 42 E. F. Pettersen, T. D. Goddard, C. C. Huang, G. S. Couch, D. M. Greenblatt, E. C. Meng and T. E. Ferrin, *J. Comput. Chem.*, 2004, 25, 1605–1612.
- 43 JMP®, Version 12.0.1 SAS Institute Inc., Cary, NC, 1989-2007.
- 44 T. K. Govindan, *Proc. Indian Acad. Sci. A*, 1956, 44, 123.
- 45 G. S. Yellol, J. G. Yellol, V. B. Kenche, X. M. Liu, K. J. Barnham, A. Donaire, C. Janiak and J. Ruiz, *Inorg. Chem.*, 2015, 54, 470–475.
- 46 F. Chiti and C. M. Dobson, *Annu. Rev. Biochem.*, 2006, 75, 333–366.
- 47 N. G. Sgourakis, Y. Yan, S. A. McCallum, C. Wang and A. E. Garcia, *J. Mol. Biol.*, 2007, 368, 1448–1457.

- 48N. G. Sgourakis, M. Merced-Serrano, C. Boutsidis, P. Drineas, Z. Du, C. Wang and A. E. Garcia, *J. Mol. Biol.*, 2011, 405, 570–583.
- 49M. Yang and D. B. Teplow, *J. Mol. Biol.*, 2008, 384, 450–464.
- 50D. Frishman and P. Argos, *Proteins-Struct. Funct. Genet.*, 1995, 23, 566–579.

Table 1: Number of conformers found for each platinum coordination mode using LowMode MD for the six ligands studied.

Coordination mode	<u>1</u>	<u>2</u>	<u>3</u>	<u>4</u>	<u>5</u>	<u>6</u>	Ratio^a
His6 δ – His13 δ	893	425	477	970	2531	1595	1.00
His6 δ – His13 ϵ	426	495	1114	423	1640	3254	1.07
His6 ϵ - His13 δ	484	468	469	680	1736	1707	0.80
His6 ϵ - His13 ϵ	995	405	434	670	1709	1556	0.84
His6 δ - His14 δ	574	411	1407	508	1204	4627	1.27
His6 δ - His14 ϵ	1570	454	513	626	3146	1152	1.08
His6 ϵ - His14 δ	429	618	404	403	1430	2118	0.78
His6 ϵ - His14 ϵ	1135	450	768	298	1226	1350	0.76
Ratio^b	1.00	0.57	0.86	0.70	2.67	2.25	

^a Ratio of the total number of conformations of a coordination mode, relative to His6 δ - His13 δ ; ^b Ratio of the total number of conformations of a ligand, relative to 1.

Table 2: Relative energy and Boltzmann factors at 310K for low energy conformations.

Ligand	Coordination	Rel. E/ kJ mol ⁻¹	Boltzmann fraction
<u>1</u>	His6 ϵ – His13 ϵ	0.00	0.79
	His6 ϵ – His13 ϵ	6.27	0.07
	His6 ϵ – His13 ϵ	7.07	0.05
	His6 ϵ – His13 ϵ	7.51	0.04
<u>2</u>	His6 ϵ – His14 ϵ	0.00	0.38
	His6 ϵ – His14 ϵ	0.77	0.28
	His6 ϵ – His14 ϵ	1.96	0.18
	His6 ϵ – His14 ϵ	4.14	0.08
	His6 ϵ – His14 ϵ	4.38	0.07
<u>3</u>	His6 δ – His13 ϵ	0.00	0.67
	His6 δ – His13 ϵ	5.80	0.07
	His6 δ – His13 ϵ	6.30	0.06
	His6 ϵ – His13 ϵ	6.45	0.05
	His6 ϵ – His14 ϵ	7.54	0.04
<u>4</u>	His6 δ – His14 δ	0.00	0.99
	His6 ϵ – His13 δ	12.69	0.01
	His6 ϵ – His13 δ	13.22	0.01
<u>5</u>	^a His6 δ – His14 ϵ	0.00	0.39
	^a His6 δ – His14 ϵ	0.31	0.34
	^a His6 δ – His14 ϵ	3.00	0.12
	^a His6 δ – His14 ϵ	5.42	0.05
<u>6</u>	^a His6 ϵ – His14 ϵ	0.00	0.47
	^a His6 ϵ – His14 ϵ	1.79	0.23
	^a His6 ϵ – His14 ϵ	2.28	0.19
	^a His6 δ – His14 δ	3.74	0.11

^a trans to 5-membered ring

Table 3: PM7 and DFT (BHandH/6-31G*-SDD) relative energies of different His binding modes in $Pt^{II}(\text{ligand})(Cl)\text{His}$ model systems.

Ligand	Nδ / Nϵ Binding	PM7 Rel. E / kJmol⁻¹	DFT Rel. E / kJmol⁻¹
<u>1</u>	δ	6.79	17.46
	ϵ	0.00	0.00
<u>2</u>	δ	7.84	9.01
	ϵ	0.00	0.00
<u>3</u>	δ	1.09	10.68
	ϵ	0.00	0.00
<u>4</u>	δ	0.00	0.00
	ϵ	19.50	21.84
<u>5</u>	$\delta 1^a$	4.08	2.75
	$\delta 2^b$	1.77	6.88
	$\epsilon 1^a$	4.26	1.85
	$\epsilon 2^b$	0.00	0.00
<u>6</u>	$\delta 1^a$	0.00	0.00
	$\delta 2^b$	25.59	12.46
	$\epsilon 1^a$	18.57	28.36
	$\epsilon 2^b$	17.22	24.20

^a trans to 5-membered ring; ^b trans to 6-membered ring

Table 4: Favoured Pt^{II} -coordination mode for each ligand system.

Ligand	Coordination mode
<u>1</u>	His6 ϵ – His13 ϵ
<u>2</u>	His6 ϵ – His14 ϵ
<u>3</u>	His6 δ – His13 ϵ
<u>4</u>	His6 δ – His14 δ
<u>5</u>	^a His6 δ – His14 ϵ
<u>6</u>	^a His6 ϵ – His14 ϵ

^a His6 coordinated trans to 5-membered ring

Table 5: Selected geometrical parameters over all conformations for each ligand (Å and °).

First line: average and standard deviation; second line: value from lowest energy conformer

Ligand	Pt-N _{Lig}	Pt-N _{His}	His-Pt-His
<u>1</u>	1.982 ± 0.005	1.966 ± 0.004	84.5 ± 1.75
	1.986 ± 0.000	1.963 ± 0.003	88.5
<u>2</u>	1.993 ± 0.059	1.967 ± 0.050	85.7 ± 3.65
	1.991 ± 0.003	1.960 ± 0.001	85.2
<u>3</u>	1.986 ± 0.005	1.966 ± 0.006	85.5 ± 2.10
	1.984 ± 0.000	1.960 ± 0.001	85.1
<u>4</u>	1.986 ± 0.031	1.967 ± 0.018	86.2 ± 2.15
	1.983 ± 0.001	1.964 ± 0.003	87.4
<u>5</u>	1.976 ± 0.037	1.968 ± 0.057	87.0 ± 2.65
	1.975 ± 0.013	1.963 ± 0.006	88.1
<u>6</u>	1.984 ± 0.040	1.965 ± 0.037	86.3 ± 2.38
	1.983 ± 0.014	1.961 ± 0.002	82.5

Table 6: Dihedral angles of the lowest energy conformations for free Aβ in addition to each

Pt(ligand) complex studied.

	Ligand							
	Free Aβ	<u>1</u>	<u>2</u>	<u>3</u>	<u>4</u>	<u>5</u>	<u>6</u>	
ϕ_{His6}	-77.63	-94.8	-130.9	-81.2	-115.9	-125.7	-88.7	
ψ_{His6}	-21.71	-49.4	-91.6	172.4	-64.0	-52.2	-27.5	
ϕ_{Asp7}	-131.10	-143.0	-67.1	-101.0	-130.5	-52.1	-149.6	
ψ_{Asp7}	-50.71	-17.3	-46.5	7.2	-34.6	177.6	-67.1	
ϕ_{Ser8}	-162.66	76.1	-152.9	-149.0	-154.5	-149.1	-99.5	
ψ_{Ser8}	6.28	-5.8	174.9	162.7	-67.2	-46.3	-76.3	
ϕ_{Gly9}	82.45	-110.3	-87.6	-80.3	101.2	-81.5	-112.6	
ψ_{Gly9}	-42.98	-68.8	159.7	81.2	11.2	4.8	-95.0	

ϕ_{Tyr10}	-86.25	-66.3	173.9	-131.7	-59.1	114.8	-126.4
ψ_{Tyr10}	-9.01	-12.5	38.9	-21.1	-25.4	32.6	73.1
ϕ_{Glu11}	70.26	-28.0	-157.3	-113.3	-99.1	77.7	-109.0
ψ_{Glu11}	11.08	-43.4	-108.8	-124.6	-10.4	55.9	-81.5
ϕ_{Val12}	-130.56	-55.5	-128.0	-101.4	74.0	-128.2	168.3
ψ_{Val12}	66.87	-5.8	-22.5	-27.6	37.3	-33.6	-30.7
ϕ_{His13}	-122.68	-67.6	-102.8	-109.8	-132.7	-116.0	-61.4
ψ_{His13}	-32.98	-19.6	-47.6	-34.6	-53.2	-10.1	-15.4
ϕ_{His14}	56.00	-111.1	-106.3	76.4	-96.1	103.1	-51.3
ψ_{His14}	17.84	-45.7	-0.2	-50.1	19.7	33.9	-30.7

Table 7: Secondary structure analysis of the low energy conformations of free A β and each Pt(ligand) system studied using STRIDE⁵⁰.

Residue	Free Aβ	Pt(1)	Pt(2)	Pt(3)	Pt(4)	Pt(5)	Pt(6)
His6	Turn	Coil	Coil	Turn	Coil	Coil	Coil
Asp7	Turn	Turn	Coil	Turn	Coil	Turn	Coil
Ser8	Turn	Turn	Turn	Turn	Coil	Turn	Coil
Gly9	Turn	Turn	Turn	Turn	Turn	Turn	Coil
Tyr10	Turn	Turn	Turn	Coil	Turn	Turn	Turn
Glu11	Turn	3,10	Turn	Coil	Turn	Turn	Turn
Val12	Coil	3,10	Turn	Coil	Turn	Turn	Turn
His13	Coil	3,10	Turn	Coil	Coil	Turn	Turn
His14	Coil	Coil	Coil	Coil	Coil	Turn	Coil

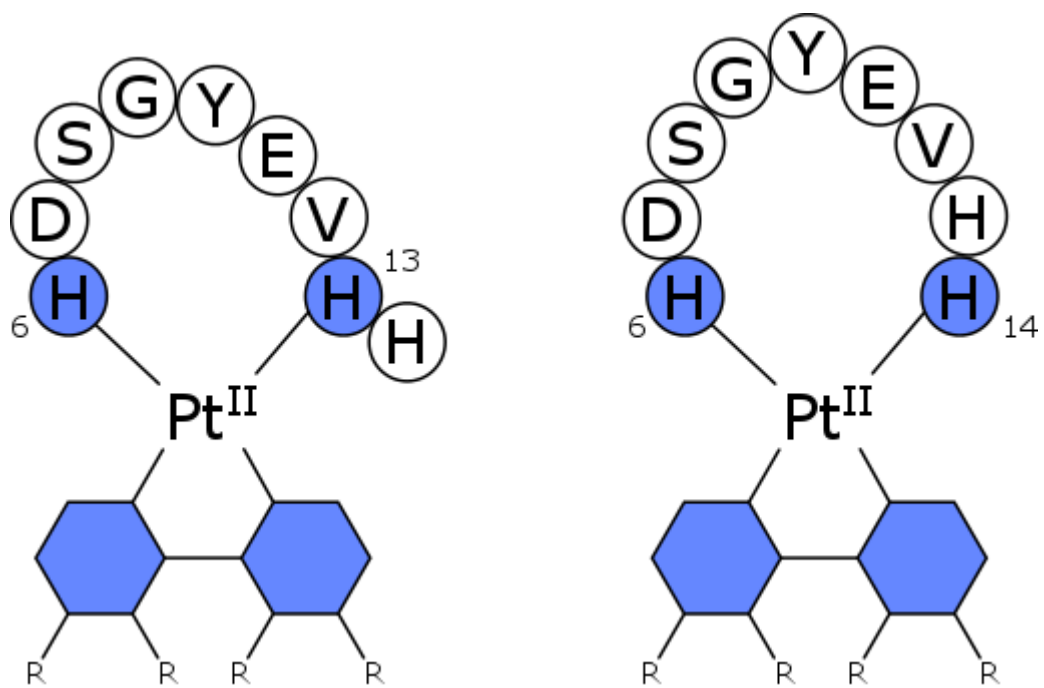


Figure 1. Schematic of Pt^{II}(ligand) binding to residues 6-14 of Aβ peptide.

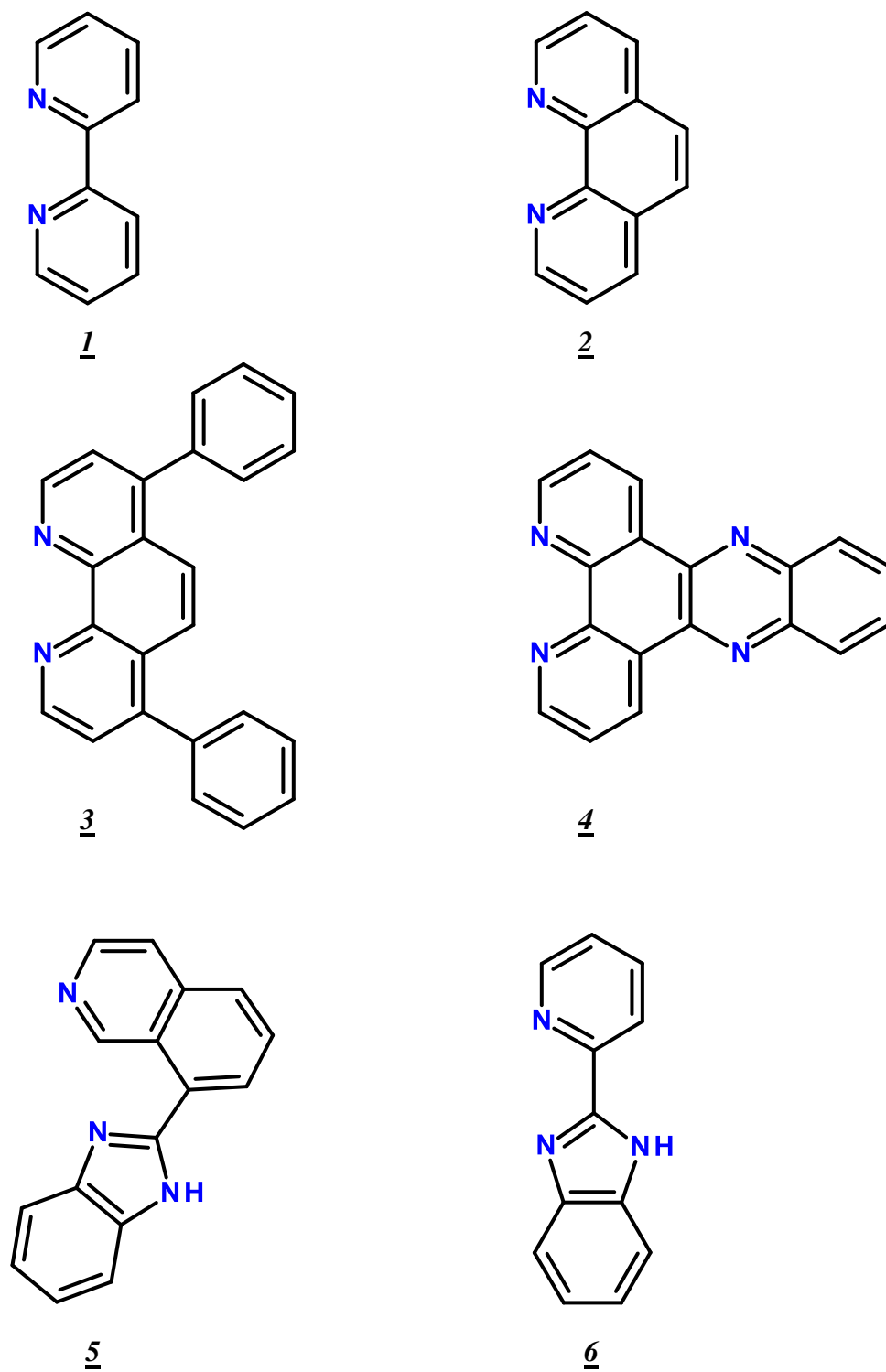
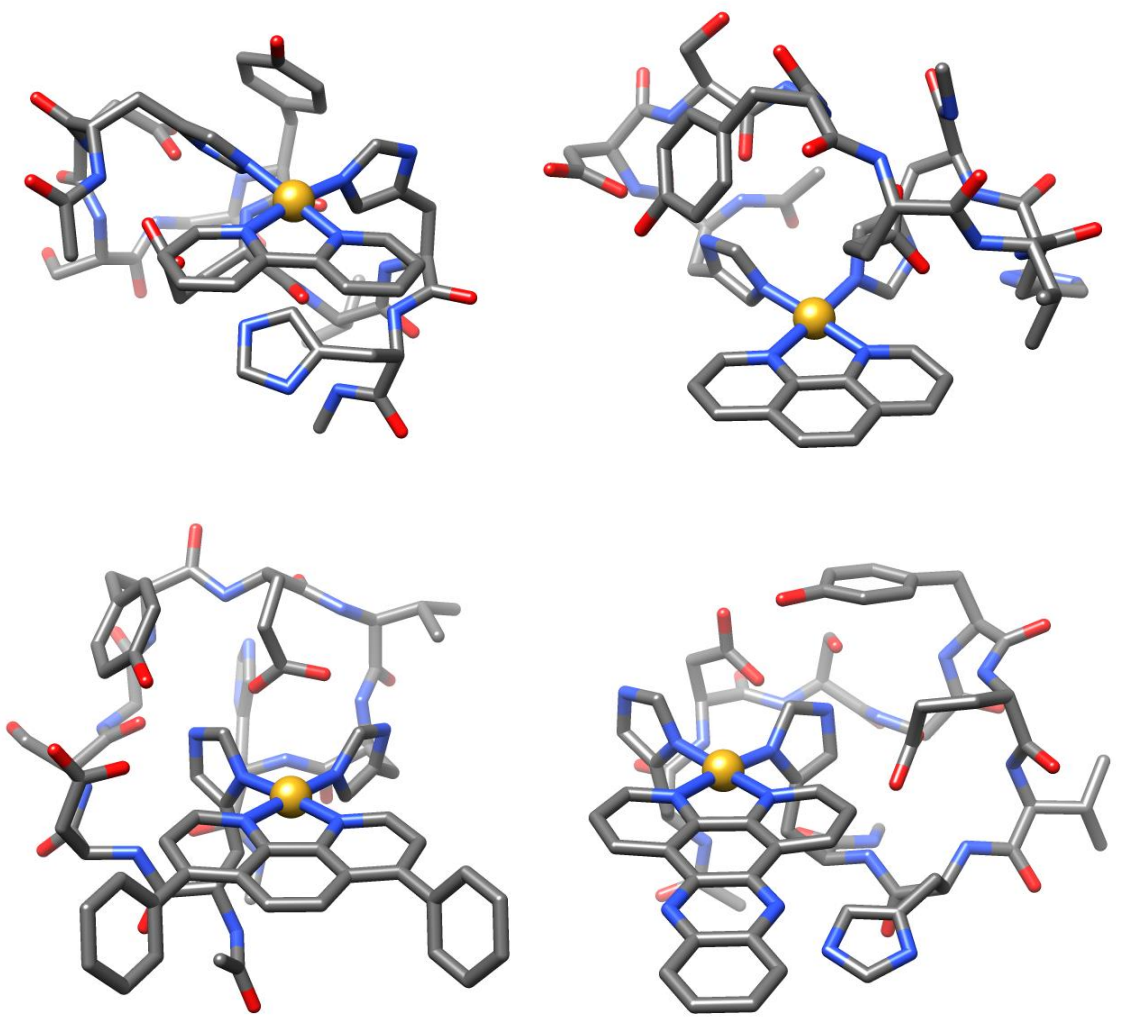


Figure 2: Schematic of ligand systems studied. (left-right: bipyridyl (1), phenanthroline (2), diphenylphenanthroline (3), dppz (4), 8-(1H-benzimidazol-2-yl)quinolone^{17,44} (5) and 2-pyridyl-benzimidazole⁴⁵ (6).



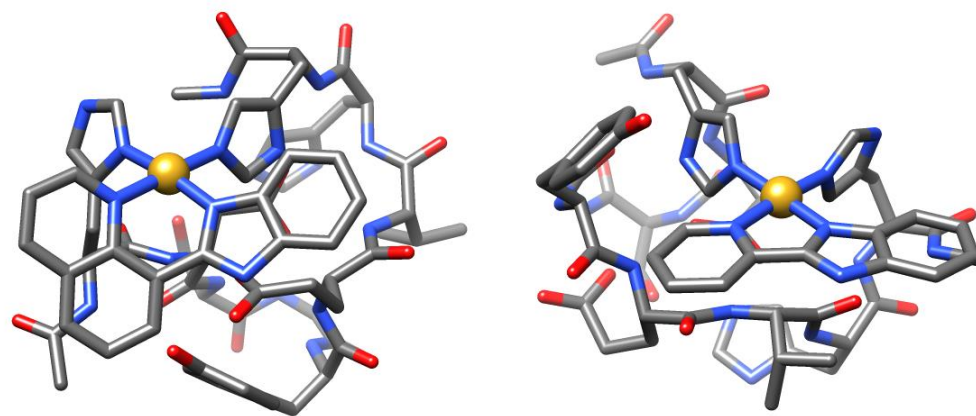


Figure 3: Top row: Low energy conformations of Pt(1) (left) and Pt(2) (right). Middle row: Low energy conformations of Pt(3) (left) and Pt(4) (right). Bottom row: Low energy conformations of Pt(5) (left) and Pt(6) (right).

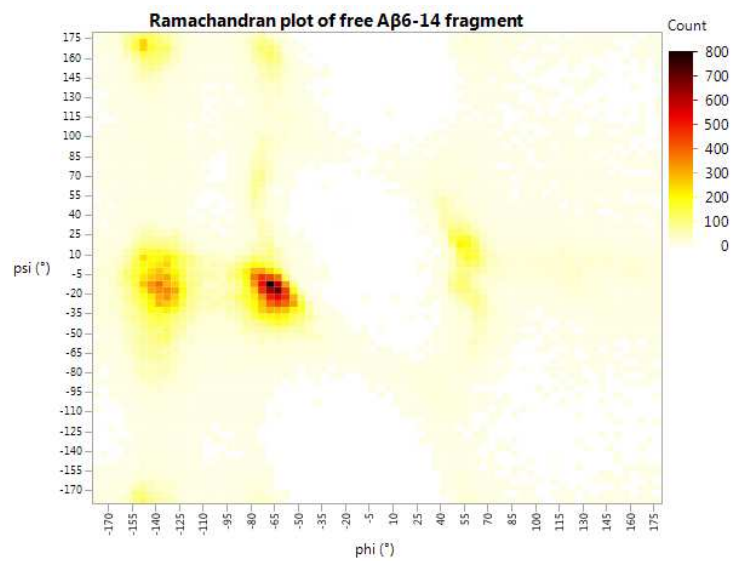


Figure 4: Ramachandran map of the generated conformations of the free $\alpha\beta$ 6-14 fragment, plotted using JMP⁴³.

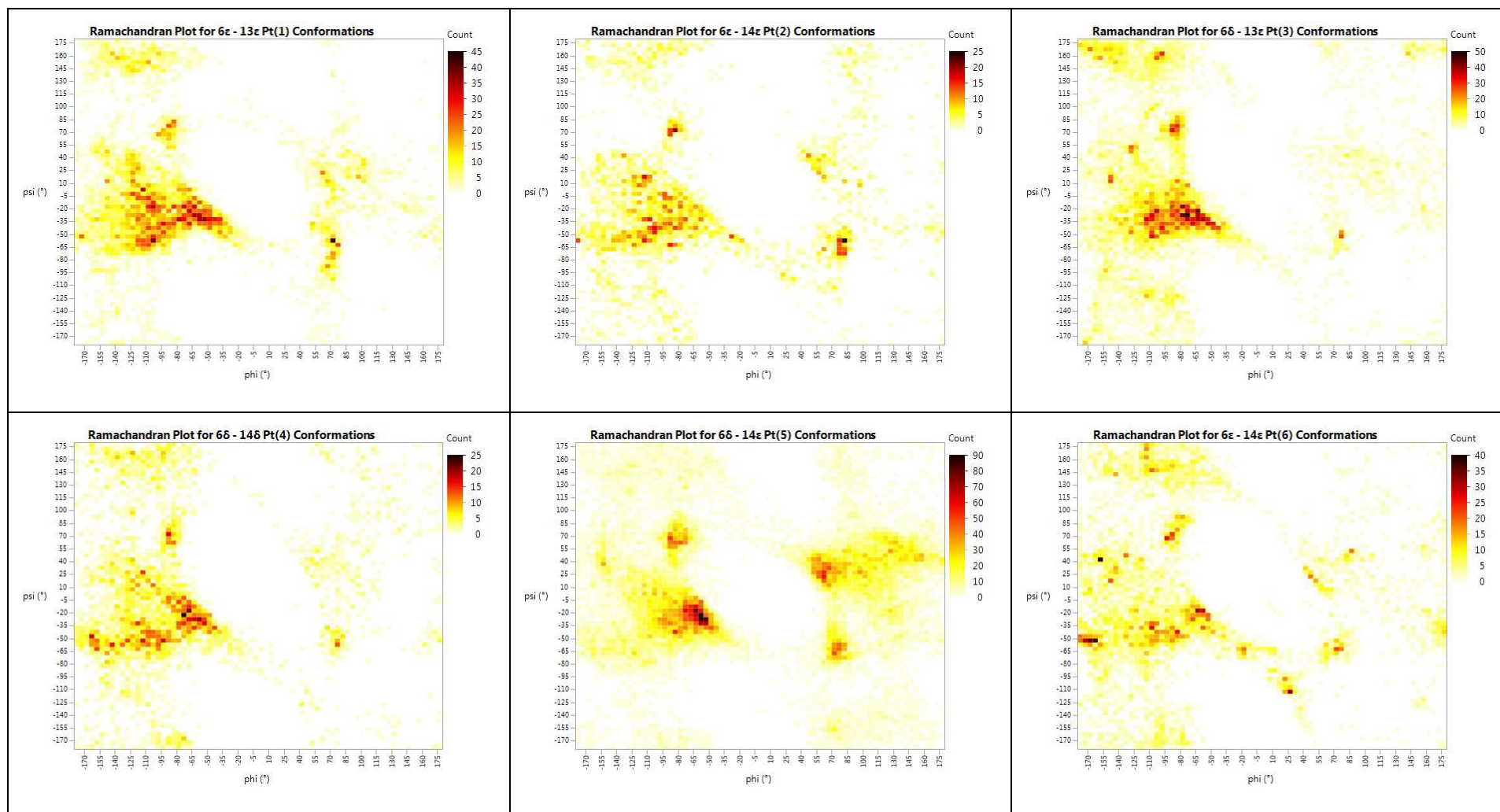
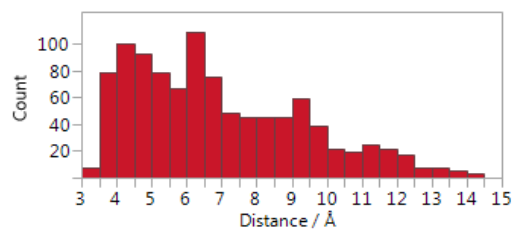
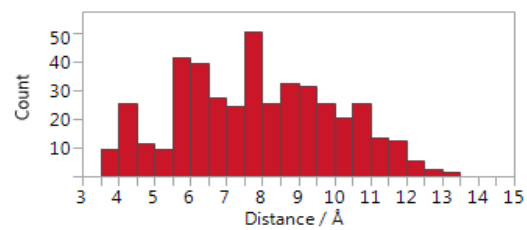


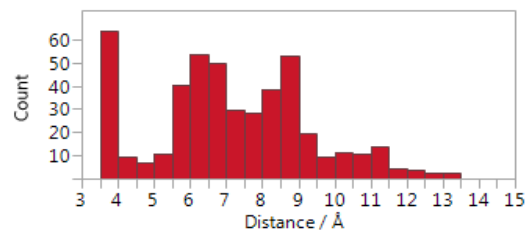
Figure 5: Comparison of Ramachandran maps for the generated conformations of the low energy binding modes for the six different Pt^{II} - $A\beta$ systems studied.



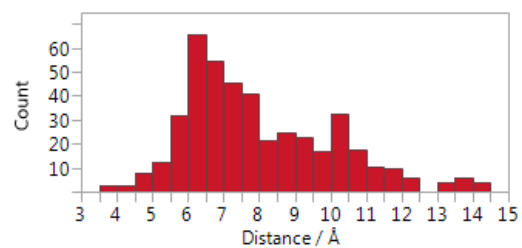
a



b



c



d

Figure 6: Ligand-Tyr10 distances in a) Pt(1) His6 ϵ - His13 ϵ , b) Pt(1) His6 δ - His13 ϵ ,
c) Pt(2) His6 ϵ - His14 ϵ and d) His6 δ - His13 δ .